IEEE Access
Multidisciplinary | Rapid Review | Open Access Journal

Received March 13, 2019, accepted April 30, 2019, date of publication May 7, 2019, date of current version May 20, 2019.

Digital Object Identifier 10.1109/ACCESS.2019.2915001

An Alternative Hybrid Time-Frequency Domain Approach Based on Fast Iterative Shrinkage-Thresholding Algorithm for Rotating Acoustic Source Identification

XIN ZHANG[1,2,3], ZHIGANG CHU[1,2], YANG YANG[1,2], SHUYI ZHAO[1,2], AND YONGXIN YANG[1,2]

[1]State Key Laboratory of Mechanical Transmissions, Chongqing University, Chongqing 400044, China
[2]College of Automotive Engineering, Chongqing University, Chongqing 400044, China
[3]Chongqing Vehicle Test & Research Institute, Co., Ltd., Chongqing 401122, China

Corresponding author: Zhigang Chu (zgchu@cqu.edu.cn)

This work was supported in part by the National Natural Science Foundations of China under Grant 11704040 and Grant 11874096, and in part by the Fundamental Research Funds for the Central Universities under Grant 2018CDQYHK0031 and Grant 2018CDXYTW0031.

ABSTRACT An alternative hybrid time–frequency domain approach based on the fast iterative shrinkage-thresholding algorithm (FISTA) is presented for rotating acoustic source identification. This approach is similar to the existing approaches based on the deconvolution approach for the mapping of acoustic sources (DAMAS) and non-negative least squares (NNLS) without the sample interpolation of sound pressure signal in the time domain. The acoustic source is first identified using the time-domain tracking Delay and Sum (DAS) method. The Frequency-domain deconvolution is then performed to attenuate the sidelobes and improve the spatial resolution. The simulation and experimental results indicate that the proposed approach is robust to the sampling rate and enjoys the good spatial convergence and resolution, effective sidelobe suppression, accurate quantification, as well as high computational efficiency. In general, at a low time-domain sampling rate, the proposed approach outperforms the DAMAS- or NNLS-based hybrid time–frequency domain approaches without the sample interpolation of sound pressure signal in the time domain.

INDEX TERMS Rotating acoustic source identification, hybrid time-frequency domain approach, fast iterative shrinkage-thresholding algorithm.

I. INTRODUCTION

Rotating beamforming is an effective noise source identification technology for rotating machines such as aero-engines [1]–[3], rotating blades [4], [5] and wind turbines [6]–[8]. Several representative frequency domain rotating beamforming techniques are as follows. Lowis and Joseph [1] proposed an in-duct focused beamformer technique using the in-duct Green's function and modal decomposition. Dougherty and Walker [2] developed a frequency domain virtual rotating microphone imaging method to locate broadband fan noise. Both methods image the rotating acoustic sources in a duct rather than in a free field. Inspired by Lowis and Joseph [1], Pannert and Maier [9] adopted the free field Green's function expressed in spherical coordinates and then expanded the application for free field. Processing in frequency domain, the above methods are convenient to construct the cross-spectral matrix and easier to use the deconvolution methods [10]–[15]. However, they are only suitable for ring arrays.

The time domain method is popular due to its wide adaptability for moving acoustic sources and applicable for different array patterns [5]–[8]. Sijtsma *et al.* [5] developed a rotating source identifier based on the time domain tracking Delay and Sum (DAS) by deriving the time domain transfer function from moving source to the static microphones. The method can effectively remove Doppler Effect caused by the movement of acoustic sources. And it can also overcome the smearing effect caused by the traditional DAS method [5]. By combining time domain tracking DAS and frequency domain deconvolution, the hybrid time-frequency domain approaches were established to obtain high-resolution imaging results [16]–[20]. Guérin and Siller [16] first proposed a hybrid time-frequency

The associate editor coordinating the review of this manuscript and approving it for publication was Md. Kamrul Hasan.

domain approach based on Deconvolution Approach for the Mapping of Acoustic Sources (DAMAS) to locate aircraft fly-over noise. Hald *et al.* [17] proposed a hybrid time-frequency domain approach based on Fourier-based Non-Negative Least-Squares (NNLS) to identify the aircraft fly-over noise. This approach was also applied for wind turbines noise source identification [18].

The above hybrid time-frequency domain beamforming approaches require a very high sampling rate to accurately determine the time delay. An inaccurate time delay estimation burdens the time domain tracking DAS with obvious deviation and the subsequent deconvolution methods with poor spatial convergence. In practice, the sample interpolation of sound pressure signal is usually performed to improve the estimation accuracy of time delay [5], [17], which however will bring large amounts of data. This requirement also appears for stationary acoustic sources [9]. In frequency domain beamforming, some scholars developed the noise source identification method based on sparsity promoting, which can effectively improve spatial resolution, convergence and robustness [21]–[23]. Lylloff *et al.* [24] proposed an efficient deconvolution method of acoustic source identification based on Fast Iterative Shrinkage-Thresholding Algorithm (FISTA) without shrinkage operator. However, they also explicitly pointed out that a sparse regularization could be used to potentially obtain a better acoustic sources identification performance in the discussion section. In this paper, inspired by [21]–[24], FISTA with sparsity promoting is applied for the rotating acoustic source identification. An alternative hybrid time-frequency domain approach based on FISTA is presented. Without the need to be sample interpolated, the original sound pressure signal is directly used for the time domain tracking DAS calculation. The proposed approach is robust to the low sampling rate and inherits the good spatial convergence and resolution, effective sidelobe suppression as well as high computational efficiency of FISTA. Especially, the proposed approach outperforms the DAMAS- or NNLS-based hybrid time-frequency domain approaches without the sample interpolation of sound pressure signal in time domain.

The rest of this paper is organized as follows: the theory of the hybrid time-frequency domain approach based on FISTA is described in Section 2. The simulations are presented in Section 3. The results of an extremely high sampling rate are given as reference. Simulations with reduced sampling rate are conducted to investigate the spatial convergence, amplitude convergence, sidelobe suppression ability. In Section 4, the simulation conclusions are verified by experiments. Finally, conclusions of this study are given in Section 5.

II. THEORY

A. HYBRID TIME-FREQUENCY DOMAIN APPROACH

The sound pressure signal in time domain perceived by the m^{th} microphone at the position $\mathbf{r}_{\mathrm{m}}$ and the reception time t is defined as $p_m(t)$, where $m = 1, 2, \ldots, M$ is the index number of the microphones and M is the total number. For the j^{th} focus point in the source plane, the output of time domain tracking DAS beamforming, $b_j(t)$, is [5], [17]:

$$\begin{cases} b_j(t) = \dfrac{1}{M}\displaystyle\sum_{m=1}^{M} \dfrac{1}{T_{mj}(\mathbf{r}_m, \mathbf{r}_j(t))} p_m(t + r_{mj}(t)/c) \\ T_{mj}(\mathbf{r}_m, \mathbf{r}_j(t)) = \dfrac{1}{4\pi \left|\mathbf{r}_m - \mathbf{r}_j(t)\right|} \end{cases} \tag{1}$$

where, $j = 1, 2, \ldots, J$ is the index number of the focus points and J is the total number, $\mathbf{r}_j(t)$ is the position of the j^{th} focus point, $r_{mj}(t)$ is the distance from the m^{th} microphone to the j^{th} focus point, and c is the sound velocity. $T_{mj}(\mathbf{r}_m, \mathbf{r}_j(t))$ is the time-dependent transfer function from the m^{th} microphone to the j^{th} focus point [5]. Since the acoustic source is moving, at each sampling time, $\mathbf{r}_j(t)$, $r_{mj}(t)$ and $T_{mj}(\mathbf{r}_m, \mathbf{r}_j(t))$ is calculated and then $b_j(t)$ can be refreshed according to Eq. (1). Note that Eq. (1) can inherently remove the Doppler effect of sound pressure signals [5], [16].

To transform the outputs of the above time domain tracking DAS to frequency domain, their autospectra $b_j(f)$ are calculated over a time data block [17]. Construct a column vector $\mathbf{b} = [b_1(f), b_2(f), \ldots, b_J(f)]^{\mathrm{T}}$, where f is frequency and the superscript "T" is the transpose operator. It is deemed belonging to the middle of the time data block. Furthermore, to visualize the acoustic sources accurately and clearly, the Point Spread Functions (PSFs) of that moment are calculated and deconvolution is then performed [17].

The core of deconvolution is to obtain the sound sources strength by removing the influence of the array PSFs from the beamforming outputs. The linear system is established as follow [10]:

$$\mathbf{b} = \mathbf{A}\mathbf{q} \tag{2}$$

where $\mathbf{q}$ is the column vector of the unknown sound source strengths, $q_j \geq 0$ is the j^{th} element of $\mathbf{q}$ and $\mathbf{A}$ is the matrix of array PSFs.

The existing hybrid time-frequency domain approaches utilize DAMAS, NNLS, etc. to solve Eq. (2) [16], [17]. DAMAS solves the source strength vector based on the Gauss-Seidel iteration [10] and NNLS based on the gradient-projection steepest descent [12].

B. FISTA

FISTA [25] is an accelerated gradient projection algorithm. The shrinkage operator for sparsity promoting is implied. In addition, it introduces a new step size and auxiliary vector making it more computationally efficient.

Eq. (2) can be transformed into the following unconstrained optimization problem [25]–[27]:

$$\hat{\mathbf{q}} = \arg\min_{\mathbf{q}} \frac{1}{2} \|\mathbf{b} - \mathbf{A}\mathbf{q}\|_2^2 + \lambda \|\mathbf{q}\|_1 \tag{3}$$

where $\hat{\mathbf{q}}$ is the optimal solution of $\mathbf{q}$, $\min(\cdot)$ denotes minimizing, $\|\cdot\|_2$ is ℓ_2 norm, $\|\cdot\|_1$ is ℓ_1 norm, and λ is the non-negative regularization parameter to promote the sparsity of acoustic sources.

When $\lambda = 0$, the sparse constraint is not used. The sound source strength is obtained by iteratively solving Eq. (3). For convenience, in this paper, this situation is denoted as $\text{FISTA}_{\lambda=0}$. When $\lambda \neq 0$, the sparse constraint is used for FISTA. The regularization parameter will promote the convergence of the results. According to lots of simulation, we set $\lambda = \min\{0.001, 0.001\,\|\mathbf{b}\|_\infty\}$, where $\|\cdot\|_\infty$ is the infinite norm.

Initialize $\mathbf{q}^{(0)} = 0$, auxiliary vector $\mathbf{y}^{(0)} = \mathbf{q}^{(0)}$ and intermediate step size $\tau^{(0)} = 1$. The lth iteration of FISTA is described as follows:

Firstly, the method uses gradient information and projects to the non-negative quadrant. The expression of $\mathbf{z}^{(l)}$ is:

$$\mathbf{z}^{(l)} = \rho_+\left(\mathbf{y}^{(l-1)} - \frac{\mathbf{A}^{\mathrm{T}}(\mathbf{A}\mathbf{y}^{(l-1)} - \mathbf{b})}{L}\right) \tag{4}$$

where ρ_+ is the Euclidean projection onto the non-negative quadrant. L is Lipschitz constant, and it is equal to the largest eigenvalue of $\mathbf{A}^{\mathrm{T}}\mathbf{A}$.

Secondly, the shrinkage operator is used to update the sound source strength $\mathbf{q}^{(l)}$ as:

$$\mathbf{q}^{(l)} = \text{sign}(\mathbf{z}^{(l)})\max\left\{\left|\mathbf{z}^{(l)}\right| - \lambda, 0\right\} \tag{5}$$

where $\text{sign}(\cdot)$ is the symbol function and $\max\{\cdot\}$ denotes maximizing.

Later, the intermediate step $\tau^{(l)}$ is updated as follow:

$$\tau^{(l)} = \frac{1 + \sqrt{1 + 4(\tau^{(l-1)})^2}}{2} \tag{6}$$

Finally, the auxiliary vector $\mathbf{y}^{(l)}$ is updated as follow:

$$\mathbf{y}^{(l)} = \mathbf{q}^{(l)} + \frac{(\tau^{(l-1)} - 1)}{\tau^{(l)}}(\mathbf{q}^{(l)} - \mathbf{q}^{(l-1)}) \tag{7}$$

The iteration is conducted until the predefined number of iterations is reached.

III. SIMULATIONS

To demonstrate the performance of the proposed approach, a simulation case study with dual rotating acoustic sources is presented in this section. The dual acoustic sources have initial positions of (0.5, 0) m and (-0.5, 0) m. They are named Source 1 and Source 2 respectively. Both sources rotate counterclockwise about the Z-axis with rotation speed of 300 r/min with a frequency of 2 kHz and strength of 100 dB. The size of source plane is 1.5 m×1.5 m The nodes of grids are focus points. The Brüel & Kjær 36-channel sector wheel array with a diameter of 0.65 m is used in the measurement. The array plane is parallel to acoustic sources plane and their distance is 1 m. A Gaussian white noise with a Signal to Noise Ratio (SNR) of 20 dB is introduced. The number of iterations is predefined as 1000 in all contour maps showing simulations. The dynamic range of display is set to 15 dB. The maximum output value is labeled on the top of each contour, and it is transformed to dB by referring to 2×10^{-5}Pa. The layout of simulation is shown as Fig. 1.

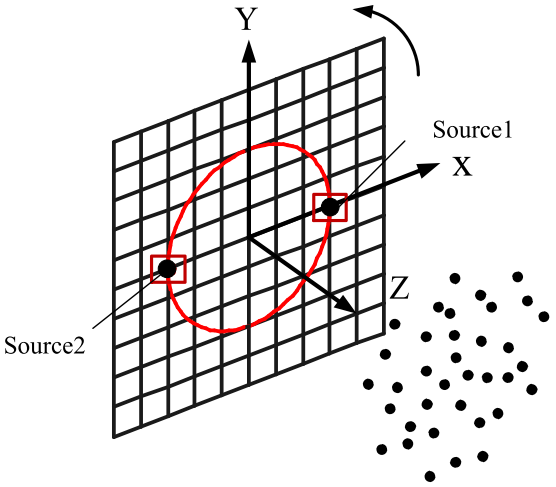

FIGURE 1. The layout schematic of simulation.

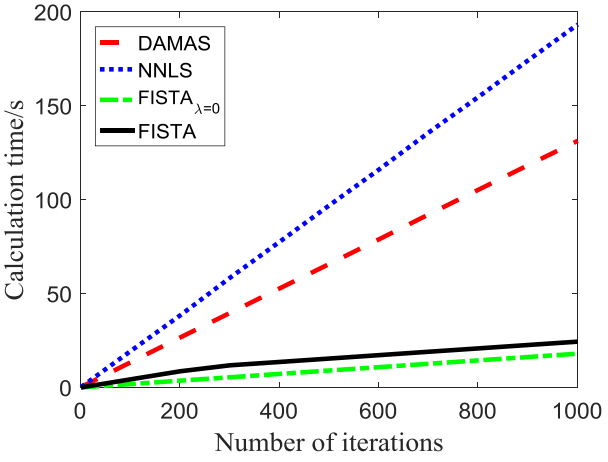

FIGURE 2. Calculation time vs. number of iterations for DAMAS, NNLS, FISTA $\lambda = 0$, and FISTA.

The sampling rate is initially set as 2^{20} Hz (1048.576 kHz). The corresponding results are treated as references. Without the need to be sample interpolated, the original sound pressure signal is directly used for the time domain tracking DAS calculation. The obtained outputs at all focus points are transformed into frequency domain by Fast Fourier Transform (FFT) and then their autospectra are obtained. The frequency resolution is 16 Hz. Table 1 shows the results from the various hybrid time-frequency domain approaches mentioned previously at the referenced sampling rate. The real source location is marked by the symbol "+". As shown, the dual acoustic sources can be distinguished using DAS method. However, the mainlobes are wide, and the spatial resolution is poor. The deconvolution methods can locate the acoustic sources precisely and the spatial resolution is greatly improved. The peak value of mainlobe is ranked in descending sequence from DAMAS, FISTA, $\text{FISTA}_{\lambda=0}$ to NNLS. Fig.2 shows the curves of calculation time vs. number of iterations for those algorithms. Clearly, the calculation efficiency of FISTA is significantly higher than that of DAMAS and NNLS. Quantitatively, at 1000 iterations, the calculation

TABLE 1. Contour maps showing simulations of acoustic sources at 2000 Hz using different methods at the referenced sampling rate.

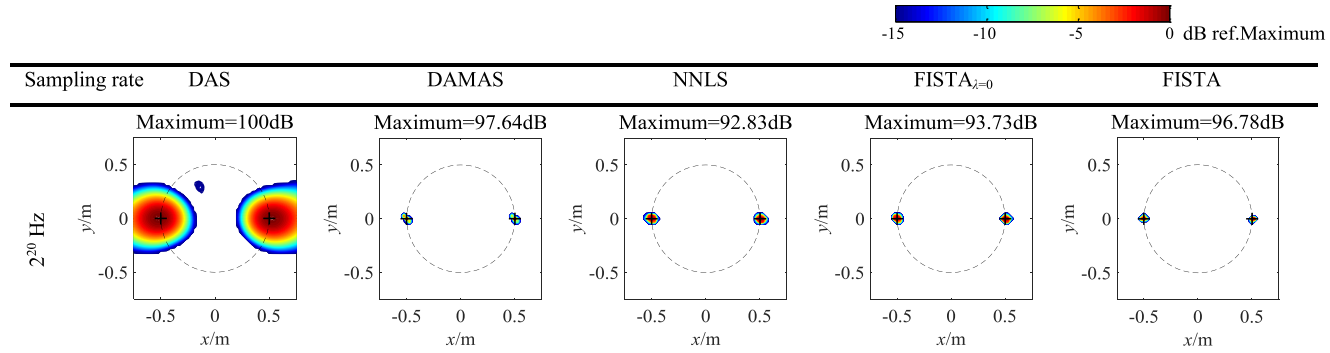

TABLE 2. Contour maps showing simulations of acoustic sources at 2000 Hz using different methods at various sampling rates.

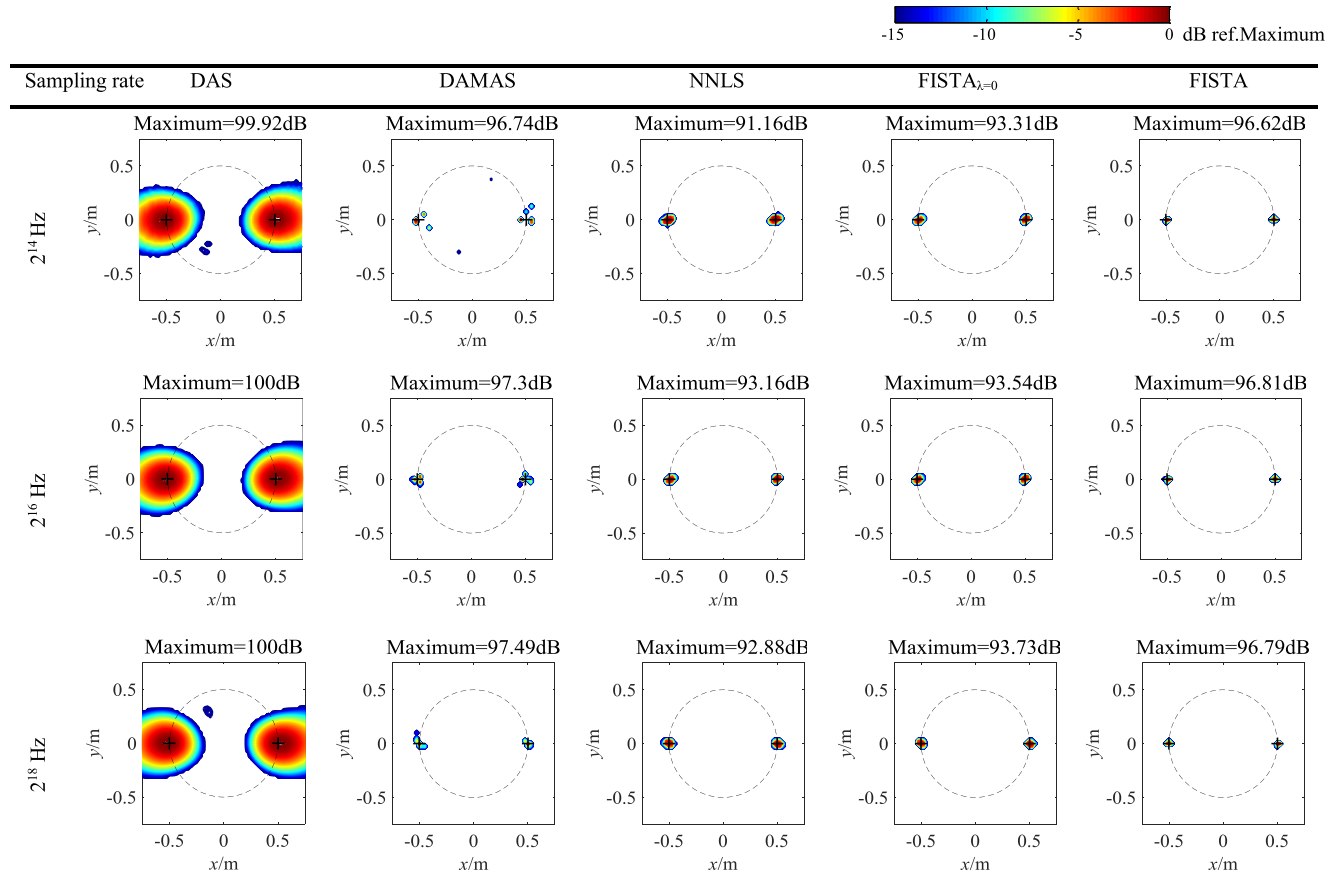

time of FISTA$_{\lambda=0}$ is 18.0 s, FISTA is 24.4 s, DAMAS is 131.3 s, and NNLS is 193.3 s. The calculation time of FISTA is about 19% of DAMAS's and 13% of NNLS's. In addition, the calculation efficiency of FISTA$_{\lambda=0}$ is slightly higher than that of FISTA, since the shrinkage operation corresponding to Eq. (5) is not performed.

In practice, the referenced sampling rate is not easy to be achieved by most data acquisition systems. Besides, high sampling rates will bring large amounts of data. Table 2 shows the acoustic source identification results of DAMAS, NNLS, FISTA$_{\lambda=0}$ and FISTA with sampling rate decreasing to 2^{14} Hz (16.384 kHz), 2^{16} Hz (65.536 kHz), 2^{18} Hz (262.144 kHz), respectively. Similar to the result at the referenced sampling rate, DAS produces wide mianlobes and little sidelobes, and the spatial resolution is poor. At two low sampling rates of 2^{14} Hz and 2^{16} Hz, the spatial convergence of NNLS, FISTA$_{\lambda=0}$ and FISTA is much better than that of DAMAS, and FISTA is best. The sources identified by DAMAS are diffused in the space. The time delay estimation error affects the performance of the hybrid time-frequency methods. The lower the used sampling rate is, the larger the time delay estimation error is, the greater the

TABLE 3. The difference between the time domain and the frequency domain DAS outputs of the static acoustic source at 2000Hz.

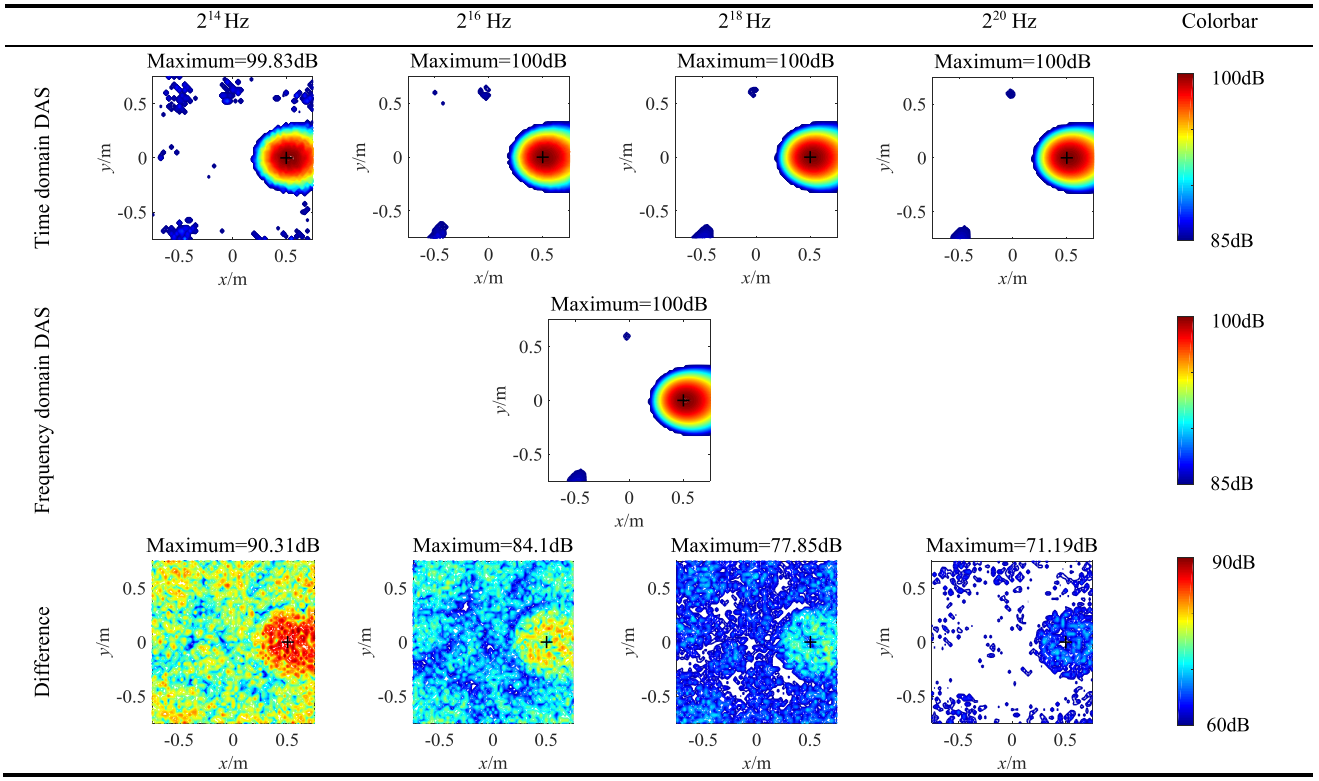

inconformity between the outputs of the time domain and the frequency domain DAS is, the worse the spatial convergence of the deconvolution results becomes. Compared with other deconvolution methods, DAMAS is most sensitive to the inconformity.

Besides, to better and intuitively display the inconformity between the frequency domain DAS and time domain DAS, a simpler case of acoustic source is presented. The Source 1 is located at the initial position of (0.5, 0) m. The frequency domain DAS and the time domain DAS are first performed respectively, and then theirs difference is getting smaller with the increase of sampling rate, as shown in Table 3. This is because the preset phase lags of frequency domain DAS among different microphone signals are the theoretical values and have nothing to do with the sampling rate. On the contrary, the preset time delays of time domain DAS among different microphone signals are integer multiples of the sampling time interval. They only approximate to the theoretical ones. In a word, the higher the used sampling rate is, the smaller the time delay estimation error is, the smaller the inconformity or error between the outputs of the time domain and the frequency domain DAS is, the better the convergence of deconvolutions is.

Fig. 3 (a)-(c) show the curves of standard deviation vs. number of iterations and Fig. 3 (d)-(f) show the curves of standard deviation vs. calculation time at various sampling rate. The standard deviation is defined as the ℓ_2 norm of the difference between the true sound sources strength vector and the reconstructed one [28]. As shown in as Fig.3 (a) (b) (d) (e), at two low sampling rates of 2^{14} Hz and 2^{16} Hz, the standard deviations of DAMAS do not reduce with the increasing of iteration number and calculation time, because the sources reconstructed by DAMAS are diffused to some focus points around the real sound source. As shown in Fig. 3 (c), at the sampling rate of 2^{18} Hz, for convergence accuracy, DAMAS is best, then FISTA, FISTA$_{\lambda=0}$ and NNLS. However, Fig. 3 (f) indicates that convergence speed of FISTA is faster than that of DAMAS.

To demonstrate the spatial convergence and quantification accuracy intuitively, Table 4 lists the peak value, the number of escape points (the focus points where portion of the source strength escapes to), and the source strength integral over the escape points. At all given sampling rates, for the differences between the reconstructed peak values and the true sound strength, DAMAS is only about 3 dB, NNLS and FISTA$_{\lambda=0}$ are higher than 6 dB, FISTA is about 3.5 dB. For the number of escape points, FISTA is always the least, followed by DAMAS, FISTA$_{\lambda=0}$ and NNLS. However, as shown in the column 3 of Table 2, sources identified by DAMAS diffuse at the sampling rates of 2^{14} Hz and 2^{16} Hz. Hence, the spatial convergence of FISTA is best at given low sampling rates. This is because FISTA is a typical sparsity promoting method. By introducing the sparse regularization parameter λ, pseudo sources are suppressed, namely, mainlobes are effectively shrunk, sidelobes are attenuated and the escape points are reduced. Consequently, the convergence is improved. For quantification accuracy, all the integral values are close to the true source strength at all given sampling rates. The difference

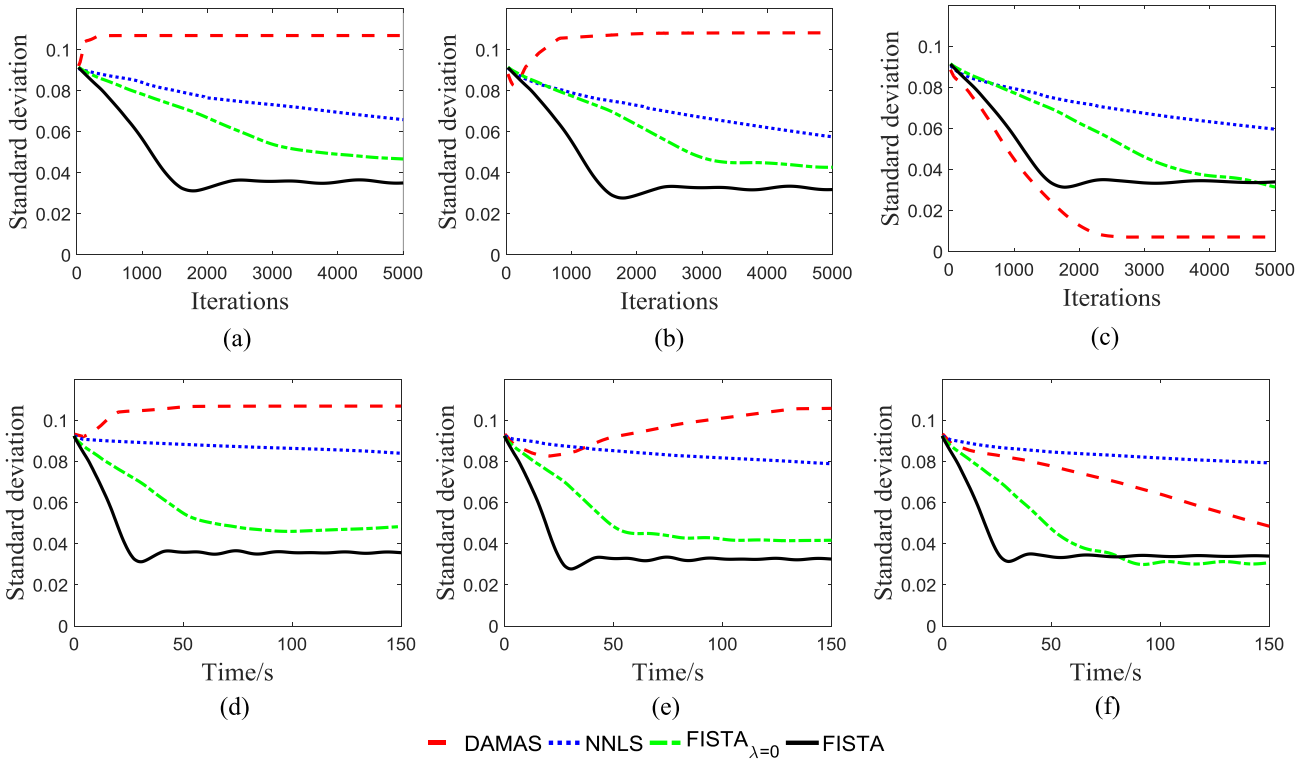

FIGURE 3. The curves of standard deviation vs. iterations (a) and time (d) at 2^{14} Hz, standard deviation vs. iterations (b) and time (e) at 2^{16} Hz, standard deviation vs. iterations (c) and time (f) at 2^{18}Hz.

TABLE 4. Simulation results of the peak value, the number of escape points, and the source strength integral at different sampling rates.

		DAMAS		NNLS		FISTA$_{\lambda=0}$		FISTA	
		Source1	Source2	Source1	Source2	Source1	Source2	Source1	Source2
2^{14} Hz	Peak value	96.71	96.74	91.15	91.16	93.03	93.31	96.62	96.57
	Point number	5	6	15	14	10	9	3	4
	Integral value	100.18	100.18	99.75	99.74	99.74	99.71	99.30	99.35
2^{16} Hz	Peak value	95.00	97.30	93.05	93.16	93.47	93.54	96.81	96.76
	Point number	6	6	10	8	10	8	4	4
	Integral value	100.04	99.99	99.94	99.84	99.93	99.90	99.58	99.56
2^{18} Hz	Peak value	97.49	97.16	92.43	92.88	93.23	93.73	96.66	96.79
	Point number	7	5	12	11	8	8	4	3
	Integral value	100.04	99.80	99.95	99.89	99.89	99.87	99.59	99.54
Reference	Peak value	97.04	97.64	92.43	92.83	93.24	93.73	96.67	96.78
	Point number	5	5	12	11	8	8	4	3
	Integral value	99.86	99.81	99.95	99.90	99.89	99.87	99.59	99.54

of FISTA is always largest, but still not exceeds 0.7 dB, which indicates that sound source strength can be accurately estimated.

In summary, at a low time domain sampling rate, compared to the hybrid time-frequency domain approaches based on DAMAS, NNLS and FISTA$_{\lambda=0}$, a better comprehensive performance of computational efficiency, spatial convergence and quantification accuracy can be achieved by the proposed approach based on FISTA.

IV. EXPERIMENT

Rotating source experiment is performed to verify the advantages of the proposed FISTA-based approach at low sampling rate. The experiment setup is shown in Fig.4. Two type HYT-3015A piezoelectric buzzers are mounted at two ends of the rotating arm, and two buzzers emit sound with strength of about 10 dB difference at 3.15 kHz. The distance from center of the buzzers to the rotating center is 0.15 m. The arm rotates counterclockwise at a speed of 375 r/min. The Brüel & Kjær

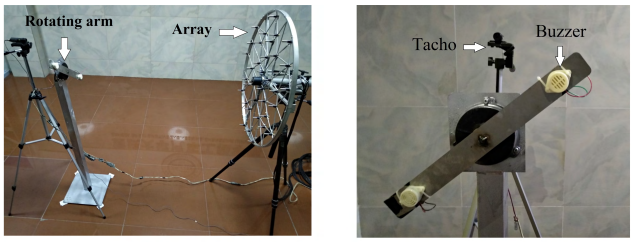

FIGURE 4. Experiment setup: (a) Measurement layout; (b) Rotating arm, tacho probe, and piezoelectric buzzers.

36-channel sector wheel array with a diameter of 0.65 m and type 2981 Tacho Probe are used. Sound pressure signals picked up by the microphones and speed pulse signal are acquired simultaneously by Brüel & Kjær 41-channel type 3560D PULSE Data Acquisition System and type 7701 Time Data Recorder. The maximum sampling frequency of system is 2^{16} Hz. The array plane is parallel to acoustic sources plane and their distance is 1 m.

The size of source plane is 0.3 m×0.3 m and the size of discretized grid is 0.01 m×0.01 m. Two experiments at sampling rates of 2^{14} Hz and 2^{16} Hz are completed respectively. Time domain tracking DAS is performed. The autospectra of the time domain tracking DAS outputs at all focus points are obtained. The frequency resolution is 16 Hz. The iteration number of deconvolution methods is 1000 and the display dynamic range is set to 15 dB.

Table 5 demonstrates the acoustic source identification results. The dotted circle in the figure is an ideal trajectory of sources, and the center of this circle corresponds to the center of the array. The contours of DAS are burdened with poor spatial resolution and serious sidelobes pollution, although it can identify dual sources. The mainlobes of DAMAS diffuse and the spatial convergence is not good enough. NNLS, $\text{FISTA}_{\lambda=0}$ and FISTA can effectively identify the acoustic sources. Compared to NNLS and $\text{FISTA}_{\lambda=0}$, the mainlobe width of FISTA is the narrowest and no sidelobes appear on its contour in the display dynamic range of 15 dB. In short, FISTA enjoys the best spatial resolution and the most effective sidelobe attenuation. In addition, there is a slight shift of sound source position in experimental results. This can be ascribed to the fact that the rotating axis of motor does not perfectly coincide with the axis of array,

TABLE 5. Contour maps showing identification results of real rotating sources at using different methods at sampling rates of 2^{14} Hz and 2^{16} Hz.

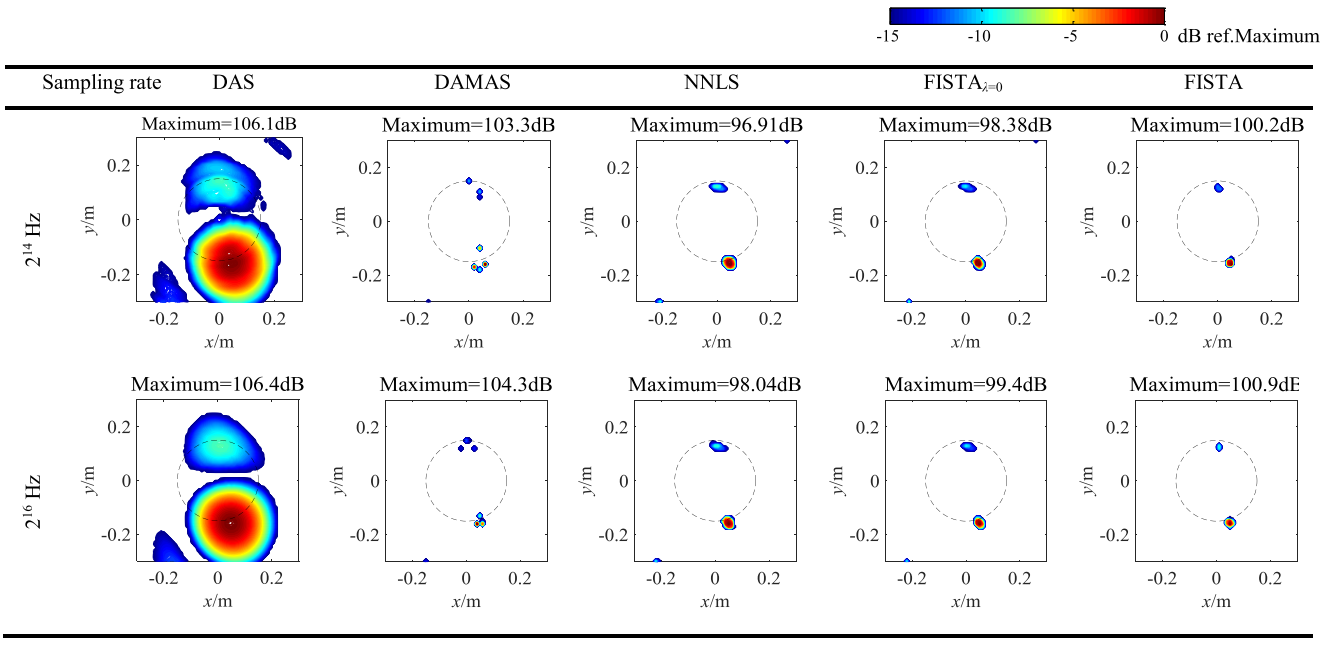

TABLE 6. Experimental results of the peak value, the number of escape points, and the source strength integral at two sampling rates.

		DAMAS		NNLS		FISTA$_{\lambda=0}$		FISTA	
		Strong	Weak	Strong	Weak	Strong	Weak	Strong	Weak
2^{14} Hz	Peak value	103.3	92.5	96.91	88.41	98.38	88.85	100.2	89.0
	Point number	Diffuse		15	11	12	10	5	3
	Integral value			105.8	96.10	105.8	96.26	105.4	93.44
2^{16} Hz	Peak value	104.3	92.10	98.04	89.24	99.40	89.90	100.9	91.7
	Point number	4	4	14	11	10	8	8	2
	Integral value	106.4	96.45	106.24	96.87	106.25	96.56	106.0	94.48

and neither pass through the midpoint of the line between the buzzers.

Table 6 lists the peak value, the number of escape points and the source strength integral to quantitively compare the spatial convergence and quantification accuracy for all deconvolution methods. Similar to simulation phenomenon, in terms of the peak value and the number of escape points, the spatial convergence performance of FISTA is superior to DAMAS, NNLS and FISTA$_{\lambda=0}$ at two sampling rates. For all deconvolution methods, the strength integral values of strong source are close. Nevertheless, that of the weak source obtained by FISTA is a little less. Therefore, how to improve its quantification accuracy of weak source is worth to study in the further work.

In general, FISTA has a better comprehensive performance than DAMAS, NNLS and FISTA$_{\lambda=0}$, which indicates that FISTA is insensitive to the error of the time domain tracking DAS outputs at low sampling rate. All conclusions are in consistence with simulation conclusions.

V. CONCLUSION

An alternative hybrid time-frequency domain approach based on FISTA is proposed for identifying the rotating acoustic sources. In general, at a low time domain sampling rate, the proposed approach outperforms the DAMAS- or NNLS-based hybrid time-frequency domain approaches without the sample interpolation of sound pressure signal in time domain. It enjoys comprehensive performance of the good spatial resolution, effective sidelobe suppression, accurate quantification and high computational efficiency. However, if the difference of source strength is too large, its quantification accuracy of the weak source needs to be improved. For further work, we are committed to seeking for solutions.

ACKNOWLEDGEMENT

The authors are deeply grateful to Dr. Liang Wang for his discussion and the people in our research group for their help in the study.

REFERENCES

[1] R. Lowis and P. Joseph, "A focused beamformer technique for separating rotor and stator-based broadband sources," in *Proc. 12th AIAA/CEAS Aeroacoust. Conf.*, May 2006, pp. 1–14.
[2] R. Dougherty and B. Walker, "Virtual rotating microphone imaging of broadband fan noise," in *Proc. 15th AIAA/CEAS Aeroacoust. Conf.*, May 2009, p. 3121.
[3] P. Sijtsma, "Using phased array beamforming to identify broadband noise sources in a turbofan engine," *Int. J. Aeroacoust.*, vol. 9, no. 3, pp. 357–374, May 2010.
[4] W. Chen and X. Huang, "Wavelet-based beamforming for high-speed rotating acoustic source," *IEEE Access.*, vol. 6, pp. 10231–10239, 2018.
[5] P. Sijtsma, S. Oerlemans, and H. Holthusen, "Location of rotating sources by phased array measurements," in *Proc. 7th AIAA/CEAS Aeroacoust. Conf. Exhib.*, May 2001, p. 2167.
[6] S. Oerlemans, P. Sijtsma, and B. M. López, "Location and quantification of noise sources on a wind turbine," *J. Sound Vib.*, vol. 299, nos. 4–5, pp. 869–883, Feb. 2007.
[7] S. Gade, J. Hald, and B. Ginn, "Noise source identification with increased spatial resolution," *J. Acoust. Soc. Amer.*, vol. 131, no. 4, pp. 9–13, Apr. 2012.
[8] S. Gade, J. Hald, J. Gomes, G. Dirks, and B. Ginn, "Recent advances in moving-source beamforming," *Sound Vib.*, vol. 49, no. 4, pp. 8–14, Apr. 2015.
[9] W. Pannert and C. Maier, "Rotating beamforming–motion-compensation in the frequency domain and application of high-resolution beamforming algorithms," *J. Sound Vib.*, vol. 333, no. 7, pp. 1899–1912, Mar. 2014.
[10] T. F. Brooks and W. M. Humphreys, "A deconvolution approach for the mapping of acoustic sources (DAMAS) determined from phased microphone arrays," *J. Sound Vib.*, vol. 294, nos. 4–5, pp. 856–879, Jul. 2006.
[11] R. Dougherty, "Extensions of DAMAS and benefits and limitations of deconvolution in beamforming," in *Proc. 11th AIAA/CEAS Aeroacoust. Conf.*, May 2005, p. 2961.
[12] K. Ehrenfried and L. Koop, "Comparison of iterative deconvolution algorithms for the mapping of acoustic sources," *AIAA J.*, vol. 45, no. 7, pp. 1584–1595, Jul. 2007.
[13] Y. Wang, J. Li, P. Stoica, M. Sheplak, and T. Nishida, "Wideband RELAX and wideband CLEAN for aeroacoustic imaging," *J. Acoust. Soc. Amer.*, vol. 115, no. 2, pp. 757–767, Feb. 2004.
[14] P. Sijtsma, "CLEAN based on spatial source coherence," *Int. J. Aeroacoust.*, vol. 6, no. 4, pp. 357–374, Dec. 2007.
[15] Z. Chu and Y. Yang, "Comparison of deconvolution methods for the visualization of acoustic sources based on cross-spectral imaging function beamforming," *Mech. Syst. Signal Process.*, vol. 48, nos. 1–2, pp. 404–422, Oct. 2014.
[16] S. Guerin and H. Siller, "A hybrid time-frequency approach for the noise localization analysis of aircraft fly-overs," in *Proc. 14th AIAA/CEAS Aeroacoust. Conf.*, 2008, p. 2955.
[17] J. Hald *et al.*, "High-resolution fly-over Beamforming using a small practical array," in *Proc. 18th AIAA/CEAS Aeroacoust. Conf.*, Jun. 2012, p. 2229.
[18] J. Gomes, "Noise source identification with blade tracking on a wind turbine," in *Proc. INTER-NOISE NOISE-CON Congr. Conf.*, Aug. 2012, pp. 5115–5126.
[19] P. Mo and W. Jiang, "A hybrid deconvolution approach to separate static and moving single-tone acoustic sources by phased microphone array measurements," *Mech. Syst. Signal Process.*, vol. 84, pp. 399–413, Feb. 2017.
[20] M. Debrouwere and D. Angland, "Airy pattern approximation of a phased microphone array response to a rotating point source," *J. Acoust. Soc. Amer.*, vol. 141, no. 2, pp. 1009–1018, Feb. 2017.
[21] A. Xenaki, P. Gerstoft, and K. Mosegaard, "Compressive beamforming," *J. Acoust. Soc. Amer.*, vol. 136, no. 1, pp. 260–271, Jul. 2014.
[22] T. Yardibi, J. Li, P. Stoica, and L. N. Cattafesta, "Sparsity constrained deconvolution approaches for acoustic source mapping," *J. Acoust. Soc. Amer.*, vol. 123, no. 5, pp. 2631–2642, May 2008.
[23] N. Chu, J. Picheral, A. Mohammad-Djafari, and N. Gac, "A robust super-resolution approach with sparsity constraint in acoustic imaging," *Appl. Acoust.*, vol. 76, pp. 197–208, Feb. 2014.
[24] O. Lylloff *et al.*, "Improving the efficiency of deconvolution algorithms for sound source localization," *J. Acoust. Soc. Amer.*, vol. 138, no. 1, pp. 172–180, Jul. 2015.
[25] A. Beck and M. Teboulle, "A fast iterative shrinkage-thresholding algorithm for linear inverse problems," *SIAM J. Imag. Sci.*, vol. 2, no. 1, pp. 183–202, Mar. 2009.
[26] Z. Tan, Y. C. Eldar, A. Beck, and A. Nehorai, "Smoothing and decomposition for analysis sparse recovery," *IEEE Trans. Signal Process.*, vol. 62, no. 7, pp. 1762–1774, Apr. 2014.
[27] S. J. Wright, R. D. Nowak, and M. A. T. Figueiredo, "Sparse reconstruction by separable approximation," *IEEE Trans. Signal Process.*, vol. 57, no. 7, pp. 2479–2493, Jul. 2009.
[28] Z. Chu, Y. Yang, and Y. He, "Deconvolution for three-dimensional acoustic source identification based on spherical harmonics beamforming," *J. Sound Vib.*, vol. 344, pp. 484–502, May 2015.

XIN ZHANG received the B.E. degree from the Chongqing University of Technology, Chongqing, China, in 2016. He is currently pursuing the master's degree with the College of Automotive Engineering, Chongqing University, Chongqing. His current research interests include acoustic source identification and array signal processing.

ZHIGANG CHU received the B.E., M.E., and Ph.D. degrees in vehicle engineering from Chongqing University, Chongqing, China, in 1999, 2002, and 2012, respectively. Since 2002, he has been with the College of Automotive Engineering, Chongqing University, where he is currently a Professor. He has published many peer-reviewed papers in his research areas. His research interests include vehicle system dynamics and control, vibration and noise control, computer aided testing theory and technology, signal processing, and source localization technology with phased sensor arrays.

YANG YANG received the B.E. degree in vehicle engineering from Chongqing University, Chongqing, China, in 2010, and the M.E. degree in power machinery and engineering from Tongji University, Shanghai, China, in 2013. She is currently pursuing the Ph.D. degree with the College of Automotive Engineering, Chongqing University. She is currently a Teacher with the Faculty of Vehicle Engineering, Chongqing Industry Polytechnic College. Her research interests include compressed sensing, array signal processing, and source localization.

SHUYI ZHAO received the B.S. degree in automotive engineering from Chongqing University, in 2016, where she is currently pursuing the master's degree. She has published a paper in the *Journal of Sound and Vibration*. Her current research interests include acoustic source identification, vehicle vibration, and noise control research.

YONGXIN YANG received the B.E. degree in mechanical engineering from the Qingdao University of Science and Technology, Qingdao, China, in 2017. She is currently pursuing the Ph.D. degree with the College of Automotive Engineering, Chongqing University, Chongqing, China. Her research interest includes array signal processing.